Microstructure and supercapacitive properties of rf-sputtered copper oxide thin films: influence of O_2/Ar ratio

B. Purusottam-Reddy · K. Sivajee-Ganesh ·
K. Jayanth-Babu · O. M. Hussain · C. M. Julien

Abstract We prepared copper oxide thin films as electrode of supercapacitors. Films of Cu–O were grown by rf-magnetron sputtering on stainless steel substrates maintained at 350 °C under different O_2/Ar ratios by keeping the sputtering pressure at ~1 Pa and rf-power at 220 W. The changes in the phase of copper oxide thin films from metallic copper to Cu_2O, Cu_2O to Cu_4O_3 and then to CuO were observed by varying O_2/Ar ratio from 1:25 to 1:1. Electrochemical impedance spectroscopy studies show a low charge transfer resistance of 0.3 Ω cm^{-2} for copper oxide thin films prepared at 1:11 O_2/Ar. The cyclic voltammetric studies exhibited a high rate ratio pseudocapacitance of 357 mF cm^{-2} at 0.5 mV s^{-1} for these copper oxide thin films with very good cycling capacitance even after 1000 cycles.

Keywords Copper oxide thin films · Sputtering · Microstructure · Supercapacitors

Introduction

Nanoparticulate metal oxide semiconductors have been studied intensely because of their interesting properties and wide-

B. Purusottam-Reddy · K. Sivajee-Ganesh · K. Jayanth-Babu ·
O. M. Hussain (✉)
Thin Film Laboratory, Department of Physics, Sri Venkateswara
University, Tirupati 517 502, India
e-mail: hussainsvu@gmail.com

C. M. Julien
Sorbonne Universités, UPMC Univ Paris 06, UMR 8234,
Laboratoire PHENIX, 75005 Paris, France

C. M. Julien
CNRS, UMR 8234, Laboratoire PHENIX, 75005 Paris, France

spread applications in heterogeneous catalysis [1], gas sensors [2, 3], Resistive Random Access Memory devices [4], magnetic storage media [5], Li-ion electrode materials [6], field emission devices [7, 8], high-temperature superconductors [9], solar cells [10] and so forth. In particular, the two main copper oxide phases which are cuprous oxide or cuprite (Cu_2O) and cupric oxide or tenorite (CuO), with band gap in the range of 1.3–2.6 eV [11], are considered to be the most important semiconductors for technological applications. Copper oxides are also important as test materials for several fundamental physical phenomena such as Bose-Einstein condensation of excitons [12]. Cu_2O crystallizes in simple cubic structure with space group $Pn3m$ and shows p-type conductivity that is attributed to the formation of Cu vacancies. On the other hand, CuO, which crystallizes in monoclinic structure with space group $C2/c$, is also a p-type semiconductor. However, a third compound is also reported in Cu–O binary system called paramelaconite (Cu_4O_3) with space group $I4_1/amd$, which have potential applications in the catalysis [13].

Due to its low cost, high chemical stability, non-toxic, abundant resources and high theoretical capacitance, copper oxide has been attracted as a promising electrode material for pseudocapacitors. Zhang et al. [14] prepared CuO with flower-like nanostructures via simple chemical deposition which displayed a specific capacitance of 133.6 F g^{-1} in KOH electrolyte. Endut et al. [15] synthesized vertical nanoflakes of copper oxide electrodes using chemical bath oxidation technique which show a specific capacity of 190 F g^{-1} in 1.0 mol L^{-1} KOH electrolyte at 2 mA cm^{-2} current density. Wang et al. [16] prepared CuO nanosheet arrays using template-free growth method which exhibited a specific capacitance of 569 F g^{-1}, with columbic efficiency higher than 93 %. Yu et al. [17] using wet-chemical process prepared 3-D porous gear-like CuO nanostructure on a Cu substrate, with specific capacitance as high as 348 F g^{-1} at a discharge current density of 1 A g^{-1}, which corresponds to the

energy density of 43.5 Wh kg^{-1}. Dubal et al. [18] reported different morphological structures of copper oxide (CuO) thin films synthesized using a surfactant-assisted chemical bath deposition method by addition of organic surfactants which exhibits a maximum specific capacitance of 411 F g^{-1} at 5 mV s^{-1}.

A variety of deposition techniques such as thermal evaporation, electrodeposition, spray pyrolysis, chemical vapour deposition, pulsed laser deposition , molecular beam epitaxy, plasma deposition and dc- and rf-magnetron sputtering have been employed for the growth of copper oxide thin films. Among these thin film deposition methods, rf-magnetron sputtering is one of the industrially practiced techniques for the preparation of uniform films on large area substrates with required chemical composition [19]. Pierson et al. [14] prepared various phases of copper oxide thin films by using rf-magnetron sputtering. Pham et al. [20] reported reactively sputtered p-type copper oxide thin films with high resistivity using Cu_2O target by varying Ar partial pressure from 0.5 to 4.0 Pa. Li et al. [21] showed single Cu_2O phase by maintaining oxygen flow rate in between 3.8 and 4.4 cm^3 min^{-1} and Ar flow rate as 40 cm^3 min^{-1} keeping rf-power at 100 W and substrate temperature at 300 °C. However, the possibility of using copper oxide films as an electrode for supercapacitor mainly depends upon the microstructure and the oxidation state, which in turn critically depends upon the deposition parameters, especially oxygen to argon ratio during sputtering.

In this work, we report the growth of copper-oxide thin films using rf-sputtering technique by varying the O_2–Ar mixture in the deposition chamber. The microstructure and surface morphology are studied as a function of the deposition parameters using X-ray diffraction (XRD), Raman spectroscopy (RS) and atomic force microscopy (AFM). The supercapacitive properties of these Cu–O thin films are examined upon 1000 cycles for different O_2/Ar ratios. We found that over a wide range of gas mixture, the composition, phase, texture and surface morphology of films strongly affect their electrochemical performance as supercapacitors (SCs). Note that the use of Cu–O electrodes and aqueous neutral electrolyte, i.e. phosphate-buffered saline (PBS), meets the requirement of "green supercapacitor" devices.

Experimental

Thin films of copper oxide were prepared from a 3″ circular copper target of 99.99 % purity on well-cleaned stainless steel substrates using rf-magnetron sputtering technique. The chamber was evacuated to a base pressure of 0.5 mPa using turbo molecular pump backed by a rotary pump. To remove the native oxide layers, the target was presputtered for 10 min by introducing argon gas into the chamber. Keeping rf-power at 220 W and substrate temperature at 350 °C, the sputtering

was carried out by admitting the oxygen and argon into the chamber through flow controllers having 0.1-sccm accuracy. During the depositions, the sputtering pressure was maintained constant at 0.94 Pa. The source to substrate distance was maintained constant at 8.0 cm. Typical deposition was carried out for 10-min duration by varying the O_2/Ar ratio, R, in the range 1:1 to 1:25.

The deposited copper oxide thin films were characterized by studying their microstructural and electrochemical properties. The structural properties were studied by Seifert X-ray diffractometer, (model 3003 TT) using CuK$_{\alpha1}$ radiation (λ= 0.15406 nm) source filtered by Ni thin film. The scan is carried out in Bragg-Brentano geometry at 0.03° s^{-1} in the 2θ range 20°–50°. The chemical composition of thin films was studied using EDAX oxford system initiated with Carl Zeiss, EVO MA 15. The local structure of Cu–O films was determined by Raman scattering (RS) spectroscopy using Labram-HR 800 confocal apparatus with He–Ne 632 nm as exiting wavelength. The surface morphology of thin films was studied using an atomic force microscope (AFM) model NT-MDT Solver Next. Electrochemical experiments were performed on a CHI 600C electrochemical workstation using three-electrode system with platinum as reference electrode with phosphate-buffered solution (PBS from Life Technologies) solution of pH 7.0 as electrolyte.

Results and discussion

Structure and morphology

Figure 1 shows the reliance of the deposition rate on the oxygen partial pressure during the rf-magnetron sputter
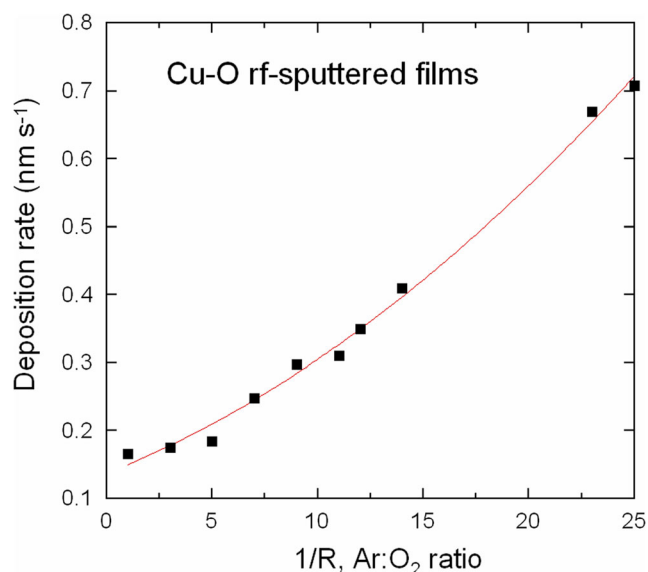

Fig. 1 Deposition rate as a function of the O_2/Ar ratio for Cu–O films grown by rf-sputtering technique

deposition of copper oxide thin films. It is observed that as R varied from 1:25 to 1:1, the deposition rate decreased from 0.7 to 0.1 nm s^{-1}. This may be ascribed to the fact that, when a metal target is exposed to discharge in a rare gas with some fraction of oxygen gas, the performance of reactive sputtering is impeded due to oxidation of metal target (poisoning). The target poisoning increases with the increase of R from 1:25 to 1:1, which results in significant reduction of sputter yield and, thus, reduced deposition rate. The thickness of the oxide layer developed on the copper target surface increases with the increase of oxygen partial pressure, which led to the decrease of the sputtering yield.

The XRD patterns of the as-deposited copper oxide thin films prepared from the Cu target at various O to Ar ratios are shown in Fig. 2. The copper oxide thin films prepared at $1:25 \leq R \leq 1:14$ exhibit a reflection at 43.31°, which corresponds to (111) orientation of FCC copper (JCPDS card no: 89-2838) which indicates copper metallic nature. For R=1:12, a weak diffraction peak was observed at 36.44° corresponding to the (111) (JCPDS card no: 78-2076) plane of cubic Cu_2O. The low intensity of the diffraction peak can be attributed to the non-stoichiometry of the Cu-rich Cu_2O film. For R=1:11, along with diffraction peak of Cu_2O (111) orientation, an additional reflection at 42.32° was observed which corresponds
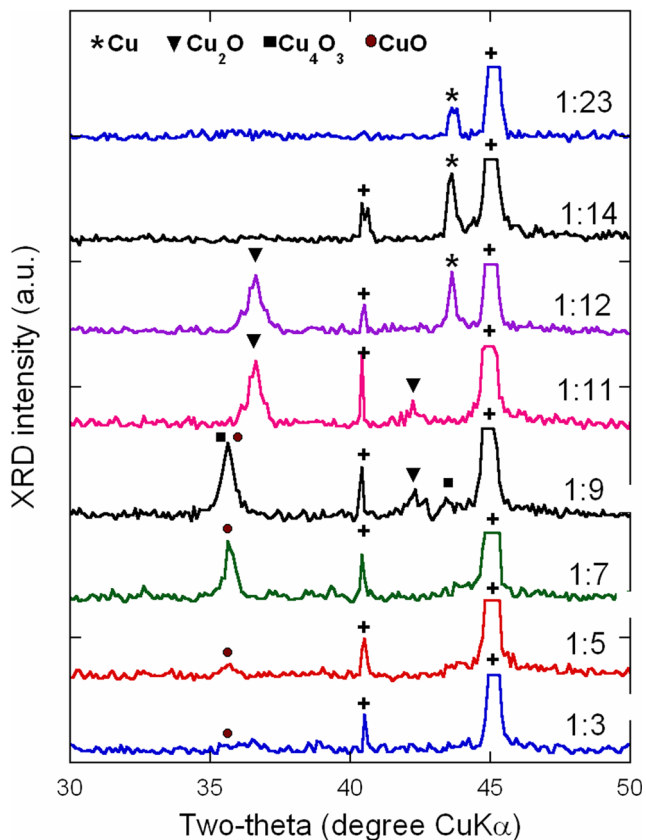
to Cu_2O (200) plane. Up on increasing R from 1:7 to 1:5, the XRD pattern shows a strong reflection at 35.55°, which corresponds to the ($\bar{1}$11) (JCPDS card no: 89-5897) reflection of monoclinic CuO phase. The crystallite size of the prepared copper oxide thin films as estimated from the Scherrer equation is given in Table 1. We observed that the grain size does not vary much with increasing R from 1:25 to 1:5. For the Cu_xO thin films prepared under R=1:3 and 1:1, the peak corresponding to ($\bar{1}$11) reflection of CuO disappears indicating the amorphous nature of the copper oxide films. As suggested by the Wang et al. [22], it is hard to determine the presence of Cu_4O_3 phase directly from XRD, as all the three phases show diffraction peaks close to 2θ=36°.

Raman scattering (RS) spectroscopy was performed to resolve the various phases Cu_2O, Cu_4O_3 and CuO present in copper oxide thin films, as the Raman active modes of these copper oxides have significant difference. Cu_2O has the cuprite structure with space group O_h^4 with two formula units per unit cell. The usual symmetry considerations predict 18 zone-centre phonon modes with symmetries $F_{2u}+E_u+3F_{1u}+A_{2u}+F_{2g}$, of which only F_{2g} mode is Raman active (gerade mode) [22–24], while copper(II) oxide belongs to the C_{2h}^6 space group with two molecules per primitive cell. There are nine zone-center optical phonon modes with symmetries $4A_u+5B_u+A_g+2B_g$, of which only three A_g+2B_g modes are Raman active [25, 26]. The paramelaconite structure group theory predicts 42 vibrational modes with symmetries $3E_g+A_{1g}+2B_{1g}+9E_u+6A_{1u}+5B_{2u}+2B_{1u}+2A_{1u}$, of which nine $3E_g+A_{1g}+2B_{1g}$ modes are Raman active [22, 25]. Figure 3 shows the RS spectra of the rf-sputtered copper oxide films prepared under R=1:14 to 1:10. One observes the characteristic phonon frequencies of the Cu_2O with additional vibrational modes apart from the characteristic Raman mode at 515 cm^{-1} deduced from the group theory. This may be due to intrinsic violation mechanism of selection rules, or the Raman scattering could be allowed through defects. The

Fig. 2 XRD patterns of copper oxide thin films deposited at different O$_2$/Ar ratios in the range 1:23 to 1:3

Table 1 Grain size, roughness and electrical resistivity of Cu_xO thin films prepared by rf-sputtering technique at different O$_2$/Ar ratios

O$_2$/Ar	Crystallite size (nm)	Grain size (nm)	Roughness (nm)	Resistivity (Ω cm)
1:3	–	20	16.2 (4)	15.12
1:5	6	35	52.6 (3)	1.73
1:7	12	52	54.1 (1)	0.68
1:9	13	54	98.1 (6)	8.1×10^{-2}
1:11	15	63	113.5 (8)	4.1×10^{-2}
1:12	12	46	73.6 (4)	1.1×10^{-3}
1:14	16	42	61.5 (2)	1.5×10^{-3}
1:23	15	53	52.6 (3)	6.8×10^{-4}

Crystallite size was determined from XRD data by the Scherrer formula, while grain size was estimated from AFM measurements
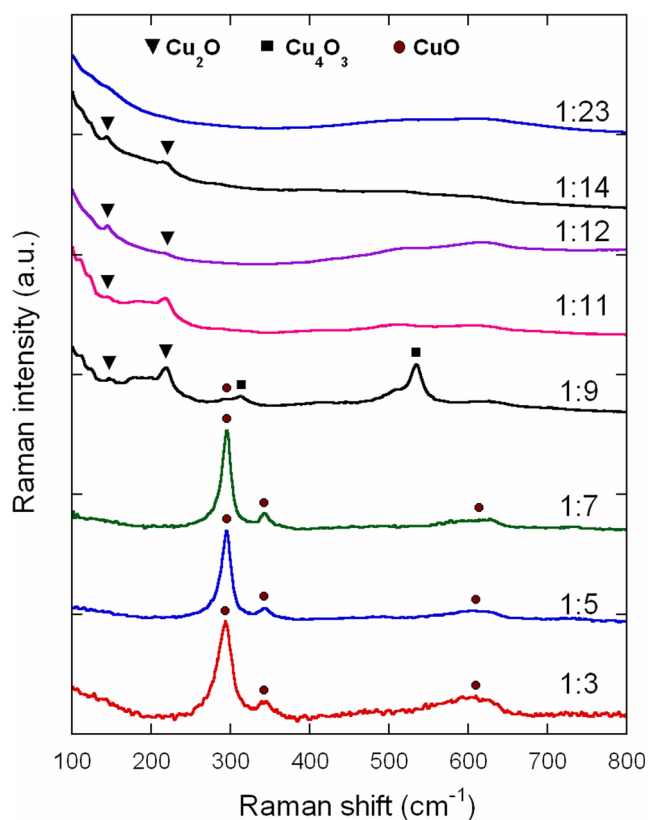
Fig. 3 Raman scattering spectra of copper oxide thin films deposited at different O_2/Ar ratios. As R increases, four phases are detected: metallic Cu, cuprite (Cu_2O), paramelaconite (Cu_4O_3) and tenorite (CuO)

strong peak at 218 cm^{-1} originated from the second-order Raman-allowed mode of the Cu_2O. The peak at 109 cm^{-1} is assigned to the inactive Raman mode. The peak at 148 cm^{-1} may be attributed to Raman scattering from phonons of symmetry F_{1u}. In addition, the weak peak located at 308 cm^{-1} corresponds to the second-order overtone mode of A_{2u} symmetry. The peak at 612 cm^{-1} is attributed to the infrared-allowed mode [23]. The Raman spectrum of thin films prepared under $R=1:7$ to 1:3 shows the characteristic peaks of CuO at 298, 330 and 602 cm^{-1} [26]. The strong peak at 298 cm^{-1} originated from the A_g Raman-allowed mode of the CuO crystals; the weak peak at 330 cm^{-1} is attributed to the B_g^1, and 602 cm^{-1} corresponds to the B_g^2 mode that is a Cu–O stretching mode. The RS spectrum of copper oxide thin films deposited at $R=1:23$ does not show any peaks confirming their metallic nature. Apart from the characteristic peaks of Cu_2O, the RS spectra of copper oxide films prepared at $R=1:9$ exhibit a most intense peak at 533 cm^{-1} and a weak peak at 312 cm^{-1}, which corresponds to A_{1g} and E_g modes of Cu_4O_3 phase, respectively. This indicates that the films prepared under this ratio grow preferably with the Cu_4O_3 phase. The peaks corresponding to Cu_2O may be due to oxidization of the unstable Cu_4O_3 phase [22]. Thus, from RS and XRD results, it is confirmed that by varying R from 1:25 to 1:1, the phase of the copper oxide films changes from metallic copper

to Cu_2O, Cu_2O to Cu_4O_3 and then to CuO. Note that the amount of oxygen available in the sputter atmosphere is the main parameter to control the structure and the composition of rf-sputtered Cu–O thin films.

The surface topography of Cu–O thin films deposited at different R values is shown in Fig. 4. The AFM results indicate that the films have grain size in 20–70-nm range. The roughness and grain size of the Cu–O films as a function of R are given in Table 1. It is observed that the roughness of the thin films increases with increase in R from 1:23 to 1:11 with a maximum value of 113 nm and, then, a further increase in R results to smaller roughness of the films. At $R=1:11$, the grains reach a critical dimension of 65 nm with high surface roughness and large specific surface area. As an experimental result, the electrical resistivity of Cu–O films increased from 6.8×10^{-4} to 15 Ω cm as R varies from 1:23 to 1:3 as shown in Fig. 5. Due to the availability of highly mobile electrons in the metallic Cu, the films deposited under oxygen-poor conditions acquire lower electrical resistivity. As the R increases from 1:25 to 1:11, the film gradually converts from metallic to semiconductor, which, in general, has high resistivity than observed in metallic bonding. Cu_2O is generally a p-type semiconductor. The p-type conduction in Cu_2O arises due to the formation of acceptor levels due to copper vacancy created in VB and is responsible for the p-type conductivity in Cu_2O [27]. In majority of metal oxide semiconductors, the states on the top of valance band are composed of O 2p states, leading to p-type conduction. These states are localized, which results in less mobility associated with poor p-type conduction. In case of Cu_2O, the states on the top of VB are dominated by completely filled $3d^{10}$ states which are not localized, i.e. more mobile when converted to holes. The electrical conductivity and hole density of p-type Cu_2O films vary with copper vacancy density, which act as shallow acceptors. With further increase of R from 1:9 to 1:3, both the XRD and Raman results indicated the formation of CuO. This led to decrease of hole density in the films and, eventually, the observed increase of the electrical resistivity of the CuO thin films. In conclusion, our results of XRD, Raman, AFM and resistivity measurements clearly show that the physical properties of the rf-magnetron-sputtered Cu–O films are highly influenced by the oxygen partial pressure that monitors the stoichiometry of these films.

Electrochemical analysis

The pseudocapacitance of rf-sputtered Cu–O films was investigated using cyclic voltammetry (CV) in a PBS aqueous solution with a three-electrode electrochemical cell. Figure 6 shows the cyclic voltammograms (CVs) of Cu–O thin films prepared at various R recorded in a potential window of 0 to -1 V with respect to platinum reference electrode at different scanning rates ranging from 1 to 10 mV s^{-1}. The CV results
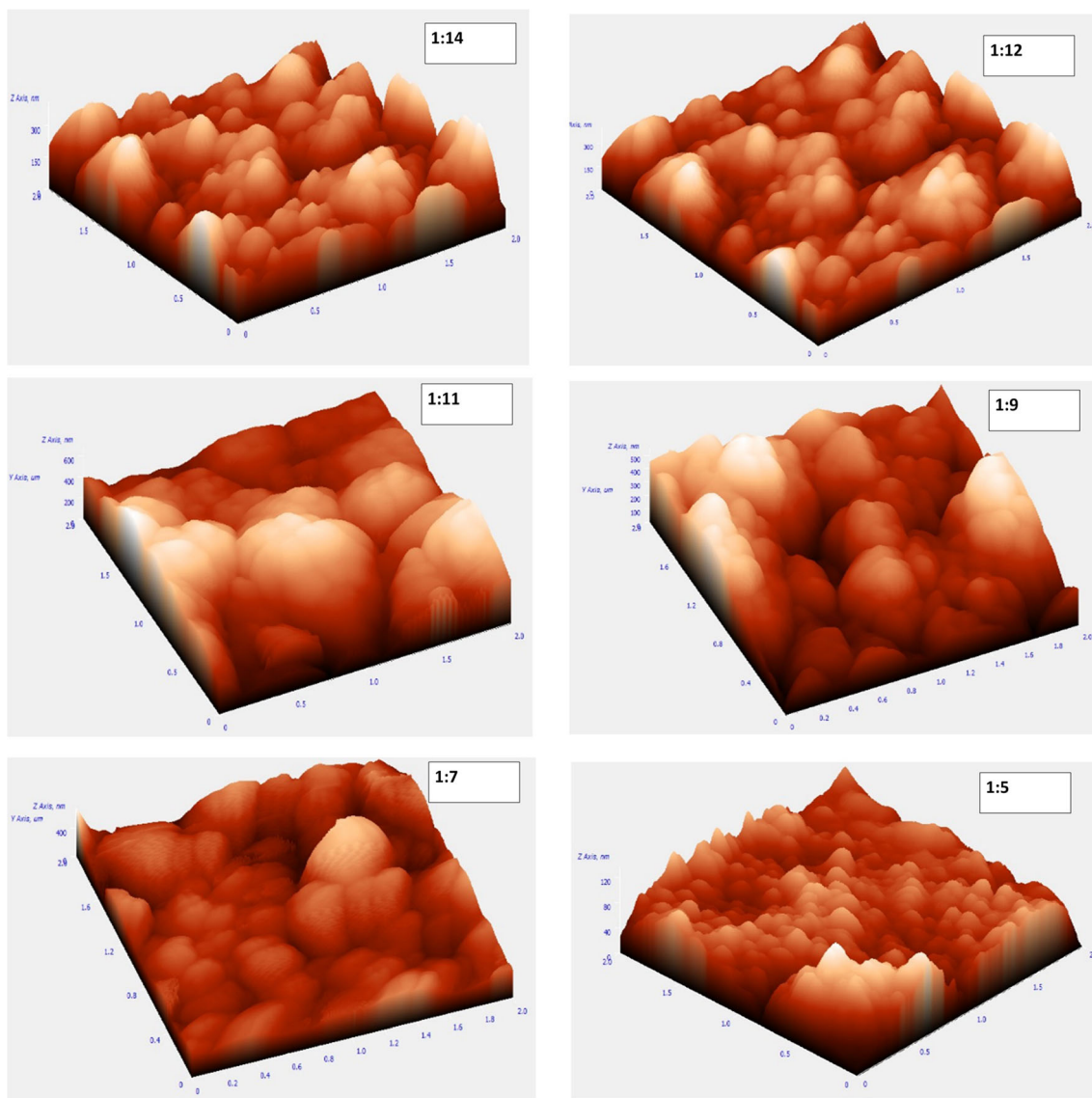
Fig. 4 Typical AFM images of copper oxide thin films deposited by rf-sputtering technique at different $R=O_2/Ar$ ratios in the range 1:14 to 1:5. It is observed that the roughness of films is strongly dependent on R: smaller roughness is obtained for higher R values

show that Faradic charge transfer processes occurred for the Cu–O films indicating a pseudocapacitance effect. Obviously, the CV is strongly dependent on the deposition conditions, i.e. composition of gas mixture and deposition rate. As pointed out by Dubal et al. [28], the shape and redox peak positions of CVs are affected by the nanostructure design of electrodes. The various curve shapes in Fig. 6 demonstrate the electrochemical response of Cu–O thin films deposited at various O_2/Ar gas ratios. The CVs of films prepared in the range $1:3 \leq R \leq 1:7$ exhibit only one anodic peak at -0.65 V and cathodic peak at -0.35 V corresponding to the formation of nonconductive, insoluble species $Cu(OH)_2$. The redox reaction towards the formation of $Cu(OH)_2$ is given by the following reaction [28–31]:

$$CuO + H_2O \leftrightarrow 2Cu(OH)_2. \qquad (1)$$

The Cu–O thin films prepared under 1:9 to 1:14 O_2/Ar ratios show two distinct anodic peaks at -0.3 and -0.65 V and two cathodic peaks at -0.15 and -0.3 V corresponding to the Cu(I)/Cu(II) redox couple and formation of $Cu(OH)_2$. In literature, this process has been described as follows [29–32]:

$$Cu_2O + 2OH^- \leftrightarrow 2CuO + H_2O + 2e^-. \qquad (2)$$
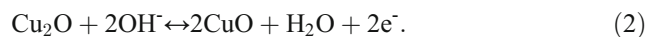
It is observed that the peak current corresponding to the Cu(I)/Cu(II) redox couple increases with the scan rate. For copper oxide thin films at $R=1:12$ apart from these peaks, there exists another cathodic peak at -0.75 V which corresponds to the reduction of CuO to Cu(III) species. According to Paixao et al. [32], for the formation of Cu(III)
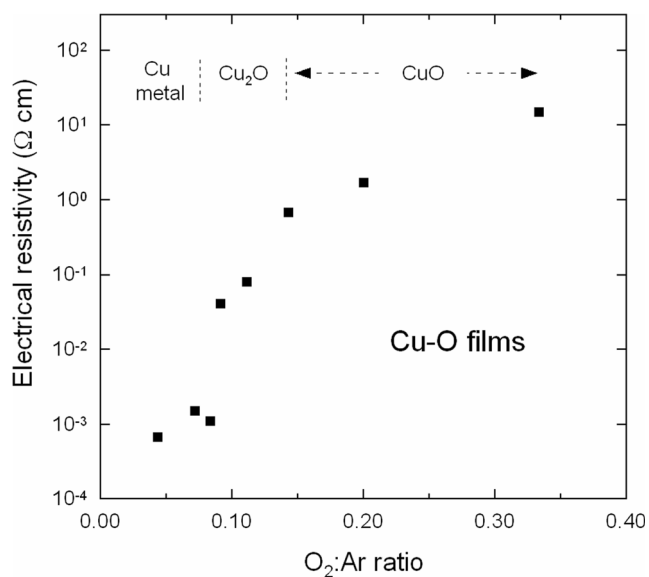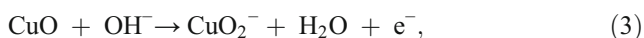
Fig. 5 Electrical resistivity of Cu–O films as a function of the O₂/Ar ratio. The Cu–O phases are marked in the range of oxygen partial pressure during rf-sputtering deposition

species, CuO was considered to be the precursor and was formed by two possible path ways:

$$CuO + OH^- \rightarrow CuO_2^- + H_2O + e^-, \qquad (3)$$

$$2CuO + 2OH^- \rightarrow Cu_2O_3 + H_2O + e^-. \qquad (4)$$

It is observed that the peak potentials vary with the thickness as well as the phase formation. As R is increased from 1:9 to 1:12, the thickness of the Cu–O films decreases and the corresponding anodic and cathodic peaks of the Cu(I)/Cu(II) redox couple shift towards lower voltages which is in good agreement with [31]. This is due to the fact that as R is increased, the ratio of Cu/O decreases and the conductivity of the oxide layer on surface of electrode changes. It is also observed that the Cu–O films prepared at $R=1:9$ does not show any observable shift in redox peaks from that of Cu₂O. This indicates the difficulty in determining the Cu₄O₃ phase using electrochemical technique. For $R=1:23$ and 1:14, i.e. copper-rich thin films, a set of two peaks appears at ca. −0.2 V which corresponds to Cu(0)/Cu(II) redox couple [29] governed by the reaction:

$$Cu + 2OH^- \rightarrow CuO + H_2O + 2e^-. \qquad (5)$$
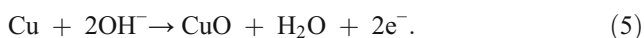
Galvanostatic charge-discharge profile of the Cu–O films carried out at current density of 0.5 mA cm⁻² in PBS solution (pH of 7.0) is shown in Fig. 7. The specific capacitance of the

prepared copper oxide thin films was calculated using the formula [15]:

$$C_s = \frac{I}{\left(\Delta V / \Delta t\right) w}, \qquad (6)$$

where C_s is the specific capacitance (F cm⁻²), I is the current (A), ΔV is the potential drop during discharge (V), Δt is the total discharge time (s), and w is the active area of the material (cm²). The calculated specific capacitance values of rf-sputtered Cu–O film electrodes prepared at $R=1:23$, 1:14, 1:12 and 1:11 at a current density of 0.5 mA cm⁻² are 220, 237, 240 and 357 mF cm⁻², respectively. For the electrodes prepared at $R=1:9$, 1:7 and 1:5, we found $C_s=325$, 147 and 103 mF cm⁻², respectively. The performance of Cu–O film electrodes in the present study is observed to be more superior than that reported for CuO films deposited by chemical bath deposition technique [33] and also for other metal oxide thin films viz. Fe₃O₄ [34] and Mn₃O₄ [35].

A sharp voltage drop is observed at the beginning of the charge and discharge profiles which is equivalent to the series resistance of the electrochemical capacitor cell. It is clear from charge curves that most of the capacitance is generated in the potential range of −0.4 to +0.5 V, corresponding to the oxidation reaction of Cu(I) to Cu(II). The discharge curves of Cu–O thin films prepared in the range of $1:23 \leq R \leq 1:11$ show two plateaus (Fig. 7) corresponding to the reduction of CuO and Cu(OH)₂ to Cu(I), which accounts for specific capacitance of the electrodes. The films prepared at 1:7 and 1:5 O₂/Ar ratios exhibit a large IR drop which is due to the large electrical resistance offered by the CuO matrix and due to the formation of less conductive Cu(OH)₂ on the surface of the film. The Cu–O thin films prepared under $1:23 \leq R \leq 1:12$, except the films prepared at $R=1:11$, show that a maximum peak current corresponds to the formation of CuO and Cu(OH)₂. This process is governed by Eqs. (1) and (5), which leads to less specific capacitance values. It is observed from CV measurements of the films prepared at $R=1:11$ that Cu(I)/Cu(II) redox reaction is the most favourable process resulting in superior specific capacity.

Electrochemical impedance spectroscopy (EIS) studies were carried out in PBS solution. The Nyquist plots of Cu–O electrodes are shown in Fig. 8. The Nyquist plot for the electrodes prepared at $R=1:3$ and 1:5 shows a larger semicircle at higher frequencies indicating a high charge transfer resistance of the electrode. The semicircles are observed to be decreased at higher frequencies as R decreased from 1:7 to 1:23 during deposition, indicating a decrease in charge transfer resistance. A very low value of 0.3 Ω cm⁻² charge transfer resistance was observed for the electrodes prepared at $R=1:11$. It is also observed that all the electrodes, except the copper
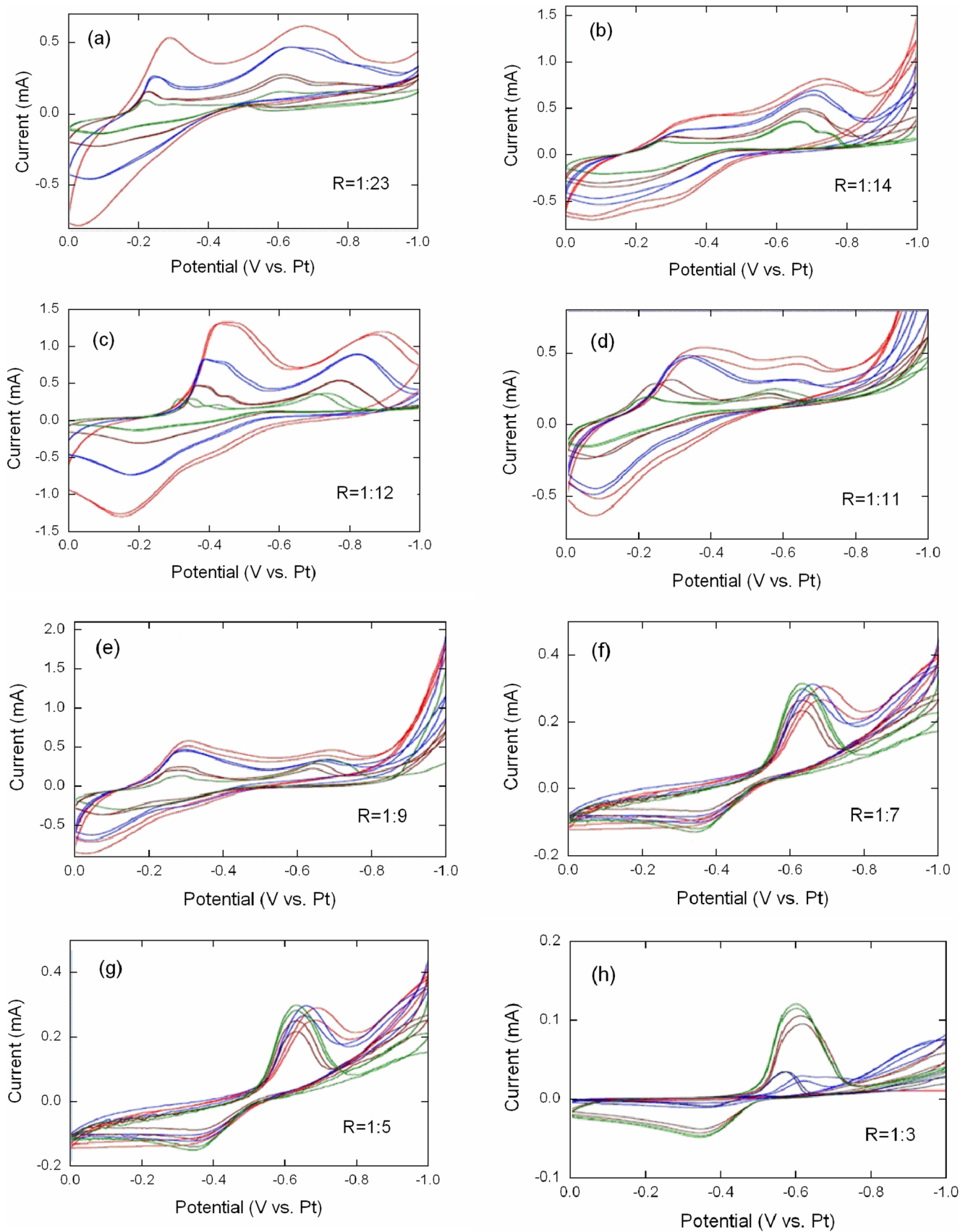
Fig. 6 Cyclic voltammograms for Cu–O thin films deposited at different O$_2$/Ar ratios, *R*, at increasing scan rates from 1 mV s^{-1} (*green curves*) to 10 mV s^{-1} (*red curves*)
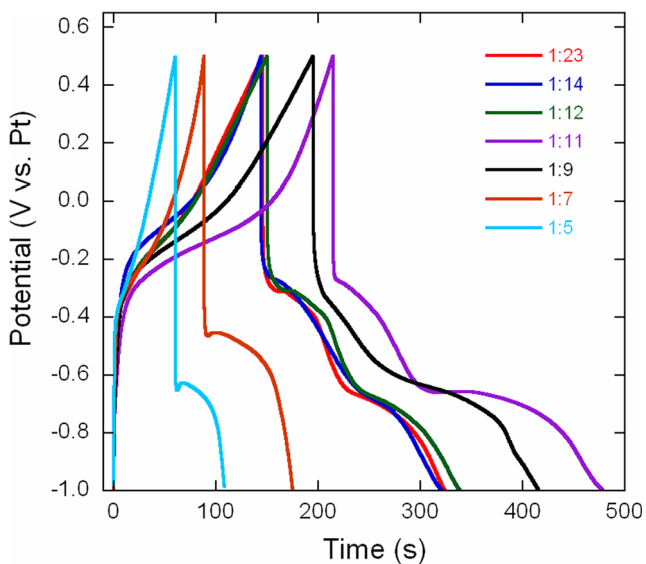
Fig. 7 Galvanostatic charge and discharge profiles of copper oxide thin films deposited at different O_2/Ar ratios at 0.5 mA cm^{-2} current density. A platinum wire was used as reference electrode and a phosphate-buffered saline (PBS) solution of pH 7 as electrolyte

oxide electrodes prepared at $R=1:11$, exhibit a nonlinear branch at low-frequency region, which indicates a larger diffusion resistance. However, the electrodes prepared at $R=1:11$ exhibit nearly a linear branch indicating the lower diffusion resistance that may be due to high surface roughness, the low resistivity and the presence of Cu_2O phase in the films. The EIS measurements clearly indicate that these films provide very low impedance and, therefore, easy redox reaction process.
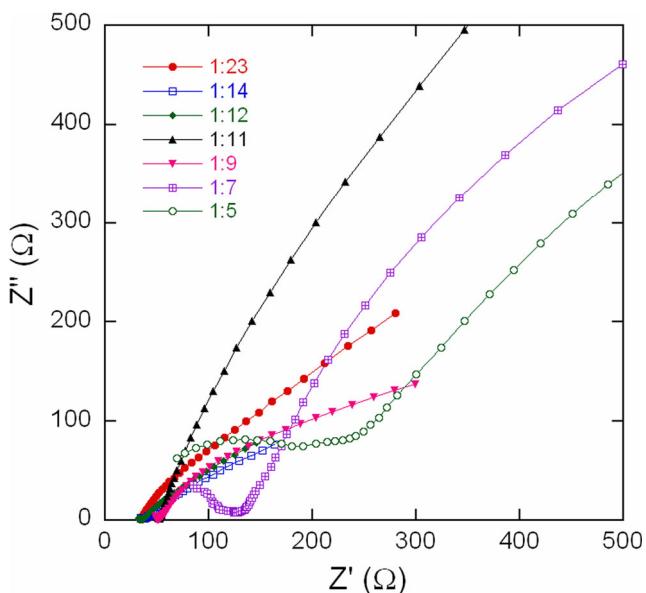
Figure 9 shows the charge-discharge profiles of copper oxide thin films prepared at $R=1:11$ as a function of current density. For 0.5–10 mA cm^{-2}, values of the specific capacitance are estimated to be 357, 262, 182, 118 and 65 mF cm^{-2}, respectively, which are comparable to the value reported by Endut et al. [15]. The substantial capacitance decrease resulting from the increase of discharge current density is likely caused by less utilization of the active electrode material for faradic redox reaction and large IR drop due to electrode resistance at high discharge current densities [16]. Figure 10 shows the cycling stability of Cu–O films prepared under various O_2/Ar ratios at 0.5 mA cm^{-2} current density. The specific capacitance decreases by a large value in early cycles due to the loss of active material caused by dissolution in the electrolyte and irreversible electrode reaction during the early cycles. After 200 cycles, all the thin films prepared under $1:14 \leq R \leq 1:9$ show good cyclability even after 1000 cycles. The films prepared under $1:7 \leq R \leq 1:5$ show less cycling stability and exhibit lowest specific capacity values (<100 mF cm^{-2}) after 500 cycles. The thin films prepared under $R=1:9$ show a large capacitive decay which may be due to conversion of Cu_4O_3 to CuO, which offers higher electrode resistance to faradic process. In particular, the films prepared under $R=1:11$ exhibit high specific capacitance and long-term stability due to open nanostructured electrode material with big grain size (65 nm) and surface roughness <100 nm that strongly enhance the reversible redox reaction process. The initial specific capacitance of 357 mF cm^{-2} decreased to 211 mF cm^{-2} after 200 cycles and retains 90 % of capacitance even after 1000 cycles. In summary, the characteristics of high specific capacitance, good rate capability and high cycling stability of mesoporous Cu_2O thin films make
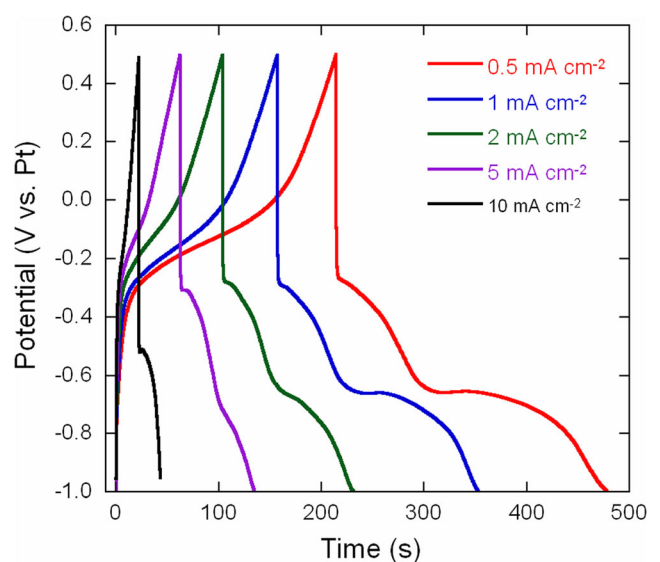

Fig. 8 Nyquist plots of copper oxide electrodes prepared at different O_2/Ar ratios in phosphate-buffered solution

Fig. 9 Galvanostatic charge and discharge profiles of copper oxide thin films deposited at 1:11 O_2/Ar ratio at different current densities
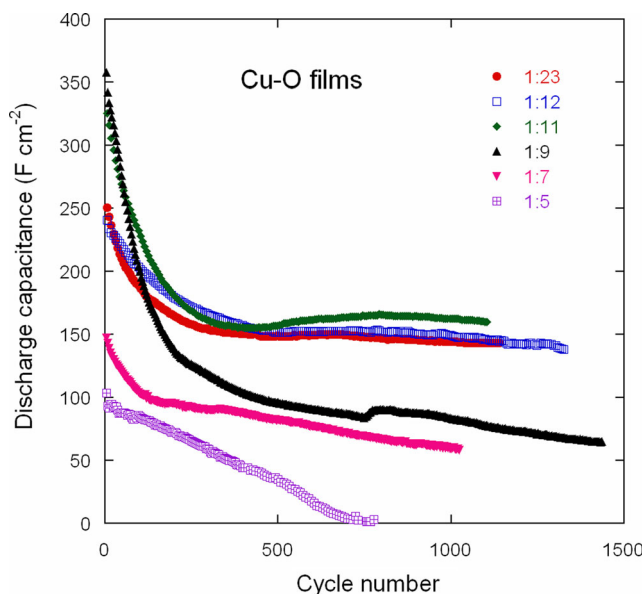
Fig. 10 Dependences of the discharge-specific capacitance of copper oxide thin films deposited at different O_2/Ar ratios on the charge/discharge cycle numbers at 0.5 mA cm^{-2} current density

them as attractive electrodes for high-performance electrochemical SCs.

Conclusion

In this work, the copper oxide thin films were deposited on stainless steel substrates using rf-magnetron sputtering technique and we studied the influence of O_2/Ar, R, during deposition on microstructural and capacitive properties. Structural properties, i.e. Raman and XRD analyses, show that by varying R from 1:25 to 1:1, the phase of the films changes into several phases from metallic copper to Cu_2O, Cu_2O to Cu_4O_3 and then to CuO. The films prepared at $R=1:11$ have high surface roughness with Cu_2O phase. The CVs show anodic and cathodic redox peaks, which are mainly from Cu(II)/Cu(I) and Cu(0)/Cu(I) redox couples. From EIS studies, a low charge transfer resistance of 0.3 Ω cm^{-2} was observed. The rf-sputtered films exhibited superior specific capacitance compared to that reported in the literature; for example, a specific capacitance of 65 mF cm^{-2} is found for a current density as high as 10 mA cm^{-2}. At current density of 0.5 mA cm^{-2}, these films displayed an initial specific capacitance of 357 mF cm^{-2} that decreased to 211 mF cm^{-2} after 200 cycles and retains 90 % of capacity even after 1000 cycles. Thus, we demonstrated that the rf-sputtering method provides copper oxide films with adequate morphology and composition for high electrochemical performance by tuning the gas mixture in the deposition chamber. These results demonstrate that rf-sputter-deposited Cu_2O thin films are good candidates as electrode material for electrochemical SC.

References

1. Zhai Q, Xie S, Fan W, Zhang Q, Wang Y, Deng W, Wang Y (2013) Photocatalytic conversion of carbon dioxide with water into methane: platinum and copper(I) oxide co-catalysts with a core-shell structure. Angew Chem 52:5776–5779. doi:10.1002/anie.201301473
2. Yang M, He J, Hu X, Yan C, Cheng Z (2013) Synthesis of nanostructured copper oxide via oxalate precursors and their sensing properties for hydrogen cyanide gas. Analyst 138:1758–1763. doi:10.1039/c2an36380a
3. Bejaoui A, Guerin J, Aguir K (2013) Modeling of a p-type resistive gas sensor in the presence of a reducing gas. Sens Actuators, B 181:340–347. doi:10.1016/j.snb.2013.01.018
4. Ogwu AA, Darma TH (2013) A reactive magnetron sputtering route for attaining a controlled core-rim phase partitioning in Cu_2O/CuO thin films with resistive switching potential. J Appl Phys 113:183522. doi:10.1063/1.4804326
5. Chand P, Gaur A, Kumar A (2013) Structural, optical and ferroelectric behavior of CuO nanostructures synthesized at different pH values. Superlattices Microstruct 60:129–138. doi:10.1016/j.spmi.2013.04.026
6. Hu C, Guo J, Wen J (2012) Hierarchical nanostructure CuO with peach kernel-like morphology as anode material for lithium-ion batteries. Ionics 19:253–258. doi:10.1007/s11581-012-0756-2
7. Hsieh CT, Chen JM, Lin HH, Shih HC (2003) Field emission from various CuO nanostructures. Appl Phys Lett 83:3383. doi:10.1063/1.1619229
8. Das S, Saha S, Sen D, Ghorai UK, Banerjee D, Chattopadhyay KK (2014) Highly oriented cupric oxide nanoknife arrays on flexible carbon fabric as high performing cold cathode emitter. J Mater Chem C 2(7):1321. doi:10.1039/c3tc31972e
9. Bourges P, Sidis Y (2011) Novel magnetic order in the pseudogap state of high-copper oxides superconductors. C R Physique 12:461–479. doi:10.1016/j.crhy.2011.04.006
10. Xiao X, Miao L, Xu G, Lu L, Su Z, Wang N, Tanemura S (2011) A facile process to prepare copper oxide thin films as solar selective absorbers. Appl Surf Sci 257:10729–10736. doi:10.1016/j.apsusc.2011.07.088
11. Sohn J, Song SH, Nam DW, Cho IT, Cho ES, Lee JH, Kwon HI (2013) Effects of vacuum annealing on the optical and electrical properties of p-type copper-oxide thin-film transistors. Semicond Sci Technol 28:015005. doi:10.1088/0268-1242/28/1/015005
12. Koirala S, Naka N, Tanaka K (2013) Correlated lifetimes of free paraexcitons and excitons trapped at oxygen vacancies in cuprous oxide. J Lumin 134:524–527. doi:10.1016/j.jlumin.2012.07.035
13. Pierson JF, Thobor-Keck A, Billard A (2003) Cuprite, paramelaconite and tenorite films deposited by reactive magnetron sputtering. Appl Surf Sci 210:359–367. doi:10.1016/s0169-4332(03)00108-9
14. Zhang H, Feng J, Zhang M (2008) Preparation of flower-like CuO by a simple chemical precipitation method and their application as electrode materials for capacitor. Mater Res Bull 43:3221–3226. doi:10.1016/j.materresbull.2008.03.003

15. Endut Z, Hamdi M, Basirun WJ (2013) Pseudocapacitive performance of vertical copper oxide nanoflakes. Thin Solid Films 528: 213–216. doi:10.1016/j.tsf.2012.09.084

16. Wang G, Huang J, Chen S, Gao Y, Cao D (2011) Preparation and supercapacitance of CuO nanosheet arrays grown on nickel foam. J Power Sources 196(13):5756–5760. doi:10.1016/j.jpowsour.2011.02.049

17. Yu L, Jin Y, Li L, Ma J, Wang G, Geng B, Zhang X (2013) 3D porous gear-like copper oxide and their high electrochemical performance as supercapacitors. Cryst Eng Comm 15:7657. doi:10.1039/c3ce40824h

18. Dubal DP, Gund GS, Holze R, Jadhav HS, Lokhande CD, Park CJ (2013) Surfactant-assisted morphological tuning of hierarchical CuO thin films for electrochemical supercapacitors. Dalton Trans 42: 6459–6467. doi:10.1039/c3dt50275a

19. Jayanth-Babu K, Jeevan-Kumar P, Hussain OM, Julien CM (2012) Influence of annealing temperature on microstructural and electrochemical properties of rf-sputtered $LiMn_2O_4$ film cathodes. J Solid State Electrochem 16:3383–3390. doi:10.1007/s10008-012-1784-6

20. Viet-Pham T, Rao M, Andreasson P, Peng Y, Wang J, Jinesh KB (2013) Photocarrier generation in CuxO thin films deposited by radio frequency sputtering. Appl Phys Lett 102:032101. doi:10.1063/1.4788680

21. Li BB, Zhu JX, Chen ZF, Shen HI, Luo J (2012) Effect of oxygen content on structural and optical properties of single Cu_2O film by reactive magnetron sputtering method. J Shanghai Jiaotong Univ (Sci) 17:523–526. doi:10.1007/s12204-012-1318-5

22. Wang Y, Ghanbaja J, Soldera F, Boulet P, Horwat D, Mücklich F, Pierson JF (2014) Controlling the preferred orientation in sputter-deposited Cu_2O thin films: influence of the initial growth stage and homoepitaxial growth mechanism. Acta Mater 76:207–212. doi:10.1016/j.actamat.2014.05.008

23. Zoolfakar AS, Rani RA, Morfa AJ, O'Mullane AP, Kalantar-Zadeh K (2014) Nanostructured copper oxide semiconductors: a perspective on materials, synthesis methods and applications. J Mater Chem C 2: 5247. doi:10.1039/c4tc00345d

24. Sander T, Reindl CT, Giar M, Eifert B, Heinemann M, Heiliger C, Klar PJ (2014) Correlation of intrinsic point defects and the Raman modes of cuprous oxide. Phys Rev B 90. doi:10.1103/PhysRevB.90.045203

25. Debbichi L, Marco de Lucas MC, Pierson JF, Krüger P (2012) Vibrational properties of CuO and Cu_4O_3 from first-principles calculations, and Raman and infrared spectroscopy. J Phys Chem C 116: 10232–10237. doi:10.1021/jp303096m

26. Litvinchuk AP, Moller A, Debbichi L, Kruger P, Iliev MN, Gospodinov MM (2013) Second-order Raman scattering in CuO. J Phys Condens Matter 25:105402. doi:10.1088/0953-8984/25/10/105402

27. Bhattacharyya SR, Reppin D, Sanguino P, Ayouchi R, Polity A, Schwarz R, Hofmann D, Meyer BK (2011) Photoconductivity study of sputter-deposited Cu_2O films. Acta Phys Pol A 120:A11–A14

28. Dubal DP, Lee SH, Kim JG, Kim WB, Lokhande CD (2012) Porous polypyrrole clusters prepared by electropolymerization for a high performance supercapacitor. J Mater Chem 22:3044–3052

29. Jayalakshmi M, Balasubramanian K (2008) cyclic voltammetric behavior of copper powder immobilized on paraffin impregnated graphite electrode in dilute alkali solution. Int J Electrochem Sci 3: 1277–1287

30. Li Q, Xu P, Zhang B, Tsai H, Zheng S, Wu G, Wang HL (2013) Structure-dependent electrocatalytic properties of Cu_2O nanocrystals for oxygen reduction reaction. J Phys Chem C 117:13872–13878. doi:10.1021/jp403655y

31. Bellakhal N, Draou K, Brisset JL (1997) Electrochemical investigation of copper oxide films formed by oxygen plasma treatment. J Appl Electrochem 27:414–421

32. Paixão TRLC, Ponzio EA, Torresi RM, Bertotti M (2006) EQCM Behavior of copper anodes in alkaline medium and characterization of the electrocatalysis of ethanol oxidation by Cu(III). J Braz Chem Soc 17:374–381

33. Dubal DP, Dhawale DS, Salunkhe RR, Jamdade VS, Lokhande CD (2010) Fabrication of copper oxide multilayer nanosheets for supercapacitor application. J Alloys Compd 492:26–30

34. Wang SY, Ho KC, Kuo SL, Wu NL (2006) Investigation on capacitance mechanisms of Fe_3O_4 electrochemical capacitors. J Electrochem Soc 153:A75–A80

35. Dubal DP, Dhawale DS, Salunkhe RR, Fulari VJ, Lokhande CD (2010) Chemical synthesis and characterization of Mn_3O_4 thin films for supercapacitor application. J Alloys Compd 497:166–170